

## RCS COMPUTATION USING A PARALLEL IN-CORE AND OUT-OF-CORE DIRECT SOLVER

D. Garcia-Doñoro<sup>1,\*</sup>, I. Martinez-Fernandez<sup>1</sup>, L. E. Garcia-Castillo<sup>1</sup>, Y. Zhang<sup>2</sup>, and T. K. Sarkar<sup>3</sup>

<sup>1</sup>Department of Signal Theory and Communications, University Carlos III of Madrid, Leganés, Madrid 28911, Spain

<sup>2</sup>School of Electronic Engineering, Xidian University, No. 2 South Taibai Road, Xi'an, Shaanxi 710071, China

<sup>3</sup>Department of Electrical Engineering and Computer Science, Syracuse University, Syracuse, NY 13244, USA

**Abstract**—Application to RCS computation of a higher order solver based on the surface integral approach is presented. The solver uses a direct method to solve the corresponding algebraic system of equations. Two versions of the solver are available: in-core and out-of-core. Both are efficiently implemented as parallel codes using Message Passing Interface libraries. Several benchmark structures are analyzed showing the reliability, performance, and versatility to run in a wide variety of computer platforms, of the solver. The results shown are illustrative of what is the maximum frequency of analysis of the structures for a given type of simulation platform.

### 1. INTRODUCTION

Radar Cross-Section (RCS) prediction is of crucial interest in military (and also civil) nautical and aeronautical industry. The use of higher working frequencies of modern radars makes RCS computation, despite the constant enhancements in computer power, a challenge, specially due to the large electrical sizes of the objects. Thus, different computer techniques for RCS prediction have been used during the last years.

Asymptotic high frequency methods, as those based either on currents (e.g., Physical Optics — PO — approximation [1], Physical

---

*Received 26 May 2011, Accepted 6 July 2011, Scheduled 14 July 2011*

\* Corresponding author: Daniel Garcia-Doñoro (dgdonoro@gmail.com).

Theory of Diffraction — PTD — [2], Stationary Phase Method — SPM — [3]) or point sources (e.g., Geometrical Theory of Diffraction — GTD — [4], its variant the Uniform Theory of Diffraction — UTD — [5], Shooting and Bouncing Rays — SBR — [6]) are fast but they are only appropriate for scatterers that are large in terms of wavelength and do not have small features. On the other hand, rigorous methods based on the discretization of partial differential equations or integro-differential equations (e.g., Method of Moments — MoM — [7], Finite Element Method — FEM — [8, 9], Finite Differences — FD — [10]) are accurate despite the features of the object and the wave propagation mechanisms involved in the electromagnetic analysis. However, their direct implementation can be computationally prohibitive in terms of CPU time and memory requirements. It is worth mentioning here the hybridization of rigorous and asymptotic high frequency methods in different forms for specific types of problems (e.g., [11–15]).

Self-restricting the scope to rigorous methods, probably MoM is the most popular method for RCS computation of large scatterers, specially for metallic structures. An intensive research/development effort has been performed in the last decade to extend MoM capabilities, either for the analysis of physically larger scatterers or to extend the maximum frequency of analysis of given structures. It is worth mentioning the use of higher order discretizations [16–18], fast techniques such as Fast Multipole Method (FMM) [19], grid approaches based on Fast Fourier Transform (FFT) (e.g., [20–24]) and those based on matrix compression. The matrix compression approaches can be further subdivided into pure algebraic approaches (e.g., based on QR factorization [25], Adaptive Cross Approximation — ACA —, [26, 27], and, in general, algorithms related to hierarchical matrices [28, 29]) and approaches in which the compression is performed through the use of block basis functions based on the physics of the specific problem to solve (e.g., Matrix Decomposition Algorithm — MDA — [30, 31], Macro Basis Functions — MBF — [32], Characteristic Basis Functions Method — CBFM — [33, 34]). Also it is worth noting the use of wavelet basis and multiresolution analysis (e.g., [35, 36]).

Most of the previous approaches are based on iterative methodologies. Although iterative type solvers allow to easily handle problems with a large number of unknowns, a preconditioner is needed with the corresponding computational overhead. For monostatic RCS the iteration process must be restarted for each excitation (although some techniques allow to accelerate the process). Direct solvers, in contrast, are robust and their computational cost is basically (in a first approximation) independent of the number of excitations (right hand sides of the matrix system of equations). This latter fact makes

direct solvers specially suited for the monostatic RCS computation.

The increase of the capabilities of the direct solvers may be based on several of the compression techniques mentioned above (e.g., see [37–39]). A different approach is to rely on techniques on the computer science side and to implement a pure MoM without any approximation/acceleration technique. In this context, the objective of the paper is to evaluate the performance of a parallel electromagnetic direct solver for RCS computation which has been developed by the authors in the last years [40–43]. Specifically, two different techniques are implemented: parallel processing [44] and out-of-core algorithms, i.e., use of hard-disk memory in addition to RAM memory.

Nowadays, processors with several cores are common even in modern single-user laptop/desktop computers. Also, access to distributed computing have become quite affordable for research/development groups. Thus, it is common to have access to a small- or mid-size cluster consisting of several multi-core computer nodes with a RAM within two and four GB per core. The parallelization of the solver in such computer systems allows to dramatically reduce the computation time and, at the same time, gives access to the distributed RAM memory of the whole cluster (in the order of hundreds of GBs). Thus, the limit on the electrical size of the structures to be analyzed can be significantly increased.

However, for very large problems the limitation is still RAM memory: the RAM memory that a research group can afford. Although RAM is getting cheaper, hard disk storage is several orders of magnitude cheaper. Then, in order to break the limit imposed by the available RAM in the system, the solution is to implement an out-of-core version of the solver [45], that uses hard disk as source of memory. The philosophy is the same as in-core case, but the matrix is written to the hard disk instead of keeping it in the RAM. Although the access time to disk is several orders of magnitude longer than the one to RAM memory, the degradation in performance of an out-of-core solver with respect to an in-core one may be reduced up to 20%–30%. The key for this result resides on the possibility for a computer with the corresponding operating system to perform I/O operations while is computing. Thus, a careful tuning between computation and I/O time slots is crucial.

In the next section, details about important aspect of this solver, such as, integral equation approach, higher-order basis functions and the mentioned parallel processing and out-of-core features, are given. Section 3 shows the numerical results of several benchmark structures. The results have been obtained running the solver on three representative computer platforms. Thus, as it will be shown,

the combination of parallel processing and in-core and out-of-core strategies, provides a great versatility to the solver being able to run on a wide variety of computer platforms, going from a single-user laptop to a supercomputer. Furthermore, the results shown are illustrative of what is the maximum frequency of analysis of the structures given the available RAM (for in-core) and available RAM and HD capacity (for out-of-core) and the type of simulation platform.

## 2. PARALLEL DIRECT SOLVER

Some details of the solver are given next; specifically, about the electromagnetic formulation, the basis functions used for its discretization, and the parallel implementation in code.

### 2.1. Formulation of the Problem

The solver is based on the solution of Surface Integral Equations (SIEs) in the frequency domain for equivalent currents over dielectric boundary surfaces and electric currents over perfect electric conductors (PECs). The set of integral equations obtained are solved by using MoM, and specifically using the Galerkin method.

The solver is able to handle inhomogeneous dielectrics categorized by a combination of various homogeneous dielectrics. Therefore, any composite metallic and dielectric structure can be represented as an electromagnetic system consisting of a finite number of finite-size linear, homogeneous and isotropic regions situated in an unbounded linear, homogeneous and isotropic environment.

Let us consider an arbitrary region  $k$  with a non-zero electromagnetic field. According to the surface equivalent theorem, the field outside region  $k$  becomes zero. Hence, the region outside region  $k$  can be homogenized with respect the region  $k$  and, then, a multiple-region problem may be decomposed into  $n$  single-region problems.

The total electric field in the region  $k$  may be expressed as a sum of scattered and incident fields as follows

$$\mathbf{E}^{(k)} = \sum_{\substack{v=0 \\ v \neq k}}^n \mathbf{E}^{(k)}(\mathbf{J}_{skv}, \mathbf{M}_{skv}) + \mathbf{E}_{inc}^{(k)} \quad (1)$$

where  $\mathbf{E}^{(k)}(\mathbf{J}_{skv}, \mathbf{M}_{skv})$  represents the scattered field inside region  $k$ , which is calculated by the currents placed on the boundary surface between regions  $k$  and  $v$ , and  $\mathbf{E}_{inc}^{(k)}$  is the corresponding incident field. The electric and magnetic scattered fields inside region  $k$  are given by

$$\mathbf{E}^{(k)}(\mathbf{J}_{skv}, \mathbf{M}_{skv}) = -L^{(k)}(\mathbf{J}_{skv}) + K^{(k)}(\mathbf{M}_{skv}) \quad (2)$$

$$\mathbf{H}^{(k)}(\mathbf{J}_{skv}, \mathbf{M}_{skv}) = -K^{(k)}(\mathbf{J}_{skv}) - \frac{\varepsilon^{(k)}}{\mu^{(k)}} L^{(k)}(\mathbf{M}_{skv}) \quad (3)$$

where  $L$  and  $K$  are linear operators given by

$$L^{(k)}(\mathbf{X}_{skv}) = j\omega\mu^{(k)} \int_{S_{kv}} \left[ \mathbf{X}_{skv}(\mathbf{r}_{kv}) g^{(k)}(\mathbf{r}, \mathbf{r}') + \frac{1}{\omega^2 \varepsilon^{(k)} \mu^{(k)}} \nabla_{skv} \cdot \mathbf{X}_{skv}(\mathbf{r}_{kv}) \nabla g^{(k)}(\mathbf{r}, \mathbf{r}') \right] \partial S_{kv} \quad (4)$$

$$K^{(k)}(\mathbf{X}_{skv}) = \int_{S_{kv}} \mathbf{X}_{skv}(\mathbf{r}_{kv}) \times \nabla g^{(k)}(\mathbf{r}, \mathbf{r}') \partial S_{kv} \quad (5)$$

with  $\mathbf{X}_{skv}$  denoting the electric or magnetic current,  $\mathbf{r}'$  is the vector position of the source point,  $\mathbf{r}$  is the vector position of the field point and  $g^{(k)}(\mathbf{r}, \mathbf{r}')$  is the Green's function for the homogeneous medium  $k$ . Making use of the boundary condition equations given by

$$\mathbf{n}_{kv} \times (\mathbf{E}^{(k)} - \mathbf{E}^{(v)}) = 0 \quad (6)$$

$$\mathbf{n}_{kv} \times (\mathbf{H}^{(k)} - \mathbf{H}^{(v)}) = 0 \quad (7)$$

and replacing (1), (2) and (3) into Equations (6) and (7), the integral equations for regions  $k$  and  $m$  are obtained in the form

$$\mathbf{n}_{km} \times \left\{ \begin{array}{l} \sum_{\substack{v=0 \\ l \neq k}}^n [L^{(k)}(\mathbf{J}_{skv}) - K^{(k)}(\mathbf{M}_{skv})] \\ - \sum_{\substack{v=0 \\ l \neq m}}^n [L^{(m)}(\mathbf{J}_{smv}) - K^{(m)}(\mathbf{M}_{smv})] \end{array} \right\} = \mathbf{n}_{km} \times (\mathbf{E}_{inc}^{(k)} - \mathbf{E}_{inc}^{(m)}) \quad (8)$$

$$\mathbf{n}_{km} \times \left\{ \begin{array}{l} \sum_{\substack{l=0 \\ v \neq k}}^n \left[ \frac{\varepsilon^{(k)}}{\mu^{(k)}} L^{(k)}(\mathbf{M}_{skv}) + K^{(k)}(\mathbf{J}_{skv}) \right] \\ - \sum_{\substack{l=0 \\ v \neq m}}^n \left[ \frac{\varepsilon^{(m)}}{\mu^{(m)}} L^{(m)}(\mathbf{M}_{smv}) + K^{(m)}(\mathbf{J}_{smv}) \right] \end{array} \right\} = \mathbf{n}_{km} \times (\mathbf{H}_{inc}^{(k)} - \mathbf{H}_{inc}^{(m)}) \quad (9)$$

These two sets of equations represent a general form of the Poggio-Miller-Chang-Harrington-Wu (PMCHW) formulation [46, 47]. When the boundary surface of two different regions is a PEC, the magnetic currents are equal to zero at the boundary surface and thus, the equations degenerates into the electric field integral equation (EFIE).

## 2.2. Higher-order Basis Functions

The electric and magnetic currents are approximated by higher order polynomials, which reduce the number of unknowns compared with the rational piece-wise basis functions. The code makes use of truncated cones for wires and bilinear patches to characterize other surfaces. Due to the type of structures analyzed in the paper, only details about the basis functions on bilinear patches are given.

For bilinear surfaces, the surface current is decomposed into its  $p$  and  $s$ -components;  $p$  and  $s$  being the two parametric coordinates of the unit quadrangle,  $p, s \in [-1, 1]$ . The approximation for the  $s$ -component of the electric current is (analogous expressions stand for the  $p$ -component and for the magnetic current)

$$\mathbf{J}_s(p, s) = \sum_{i=0}^{N_p} \left[ c_{i1} \mathbf{E}_i(p, s) + c_{i2} \mathbf{E}_i(p, -s) + \sum_{j=2}^{N_s} a_{ij} \mathbf{P}_{ij}(p, s) \right] \quad (10)$$

where  $N_p$  and  $N_s$  are the degrees of the approximations along the coordinates, and  $a_{ij}$ ,  $c_{i1}$  and  $c_{i2}$  are the unknown coefficients.

Thus, expression (10) stands for the representation of the current in terms of *edge basis functions*  $\mathbf{E}_i(p, s)$  and interior or *patch basis functions*  $\mathbf{P}_{ij}(p, s)$  which can be compactly expressed as

$$\mathbf{E}_{ik}(p, s) = \frac{\alpha_s}{|\alpha_p \times \alpha_s|} \begin{cases} p^i N(s), & k = 1 \\ p^i N(-s), & k = 2 \end{cases} \quad (11)$$

$$\mathbf{P}_{ij}(p, s) = \frac{\alpha_s}{|\alpha_p \times \alpha_s|} p^i S_j(s) \quad (12)$$

$$N(s) = \frac{1-s}{2}, \quad S_j(s) = \begin{cases} s^i - 1 & i \text{ is even} \\ s^i - s & i \text{ is odd} \end{cases} \quad (13)$$

where symbols  $\alpha_s$ ,  $\alpha_p$  denote the unitary vectors along the transformed  $s$  and  $p$  coordinates.

Edge basis functions  $\mathbf{E}_{i1}$  and patch basis functions  $\mathbf{P}_{ij}$  are zero along the first edge ( $s = -1$ ); being  $\mathbf{E}_{i2}$  and  $\mathbf{P}_{ij}$  zero along the second edge ( $s = 1$ ). Thus, the continuity equation can easily be imposed on a given mesh made of patches. Note that the code also supports other geometrical elements and bases; for further details see [48].

## 2.3. Parallel Processing and Out-of-core Techniques

The parallel implementation of an integral equation code involves parallel matrix filling followed by a parallel solution of the dense matrix

equation. Load-balancing in terms of data and CPU operations is crucial to achieve speedups with a large number of processors.

The matrix solution is based on the LU factorization algorithm. The type of solution algorithm largely influences the parallel filling strategy. In order to provide an efficient implementation, the nature of the basis functions used must be also taken into account in the filling process. Special care is needed when dealing with higher order basis. Thus, redundant computations have been eliminated as much as possible; for instance, the computation of the values of the Green's functions for the integration points of two given patches are reused. The intermediate results obtained in evaluating the elements of the impedance matrix for lower-order can be used in the computation of the elements of the impedance matrix when using higher-order polynomials. The parallel implementation is achieved by using MPI (Message Passing Interface) [49]. MPI generates a logical rectangular process grid which is assumed to map matrix data blocks onto processors. Specifically, a block-cyclic matrix distribution is used among processors as ScaLAPACK does. ScaLAPACK library [50] is used to solve the matrix system of equations.

As mentioned in the Introduction, an out-of-core version of the parallel solver has been implemented in order to break the limit imposed by the available RAM in the system. The out-of-core solver uses hard disk as source of memory. It partitions the matrix in *slabs*, the number of slabs being dependent on the relation between available hard disk storage, the RAM and the number of processors. At a rough level, it can be said that for each slab the algorithm is exactly the same as the in-core version. Obviously, the main difference is that, once a slab has been processed the data is written to disk instead of keeping it in RAM. However, there are a number of specific issues with the out-of-core solver that are worth mentioning: *left-looking* or *right looking* data access strategies, pivot policies, the possibility of recovery from a failure (due to the large wall time that can be involved in the solution of very large problems — days, or even weeks), etc.. Although the data access to disk is much slower than the access to RAM memory, the degradation in performance of the out-of-core solver with respect to the in-core may be reduced up to 20%–30%. This is achieved by overlapping the disk access operations related with the future computations with the current computational process.

Figure 1 shows the speed-up of the in-core and out-of-core solvers for one of the benchmarks performed; specifically, the monostatic analysis of the metallic NASA almond at 9.92 GHz. The speed-up on the ordinate axis represents the ratio between the execution time of the benchmark using one process (sequential execution) and the execution

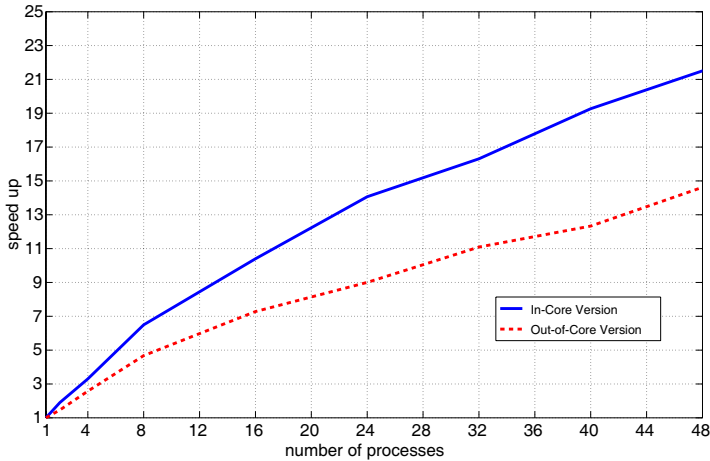


**Figure 1.** Speed-up of the *in-core* and *out-of-core* solvers for the monostatic analysis of the metallic NASA almond at 9.92 GHz.

time of the same benchmark using  $n$  processes. A linear speed-up is representative of a good scalability of the algorithm/code. The ideal situation is when the slope of the linear speed-up is one, meaning that the execution time of the parallel version is  $n$  times lower than the sequential execution time. In the figure, it is observed that, once the number of processes is higher than a few, the slopes of the speed-up curves of the in-core and out-of-core solvers are basically the same. That means that the scalability shown by both versions of the solver are similar. It is observed that the slope is not one, but around 45%–60%, which is within the expected values of a direct solver. The only significant difference between both versions of the solver is the (limited) degradation in performance of the out-of-core solver with respect to the in-core, as it was mentioned above.

### 3. NUMERICAL RESULTS

To illustrate the performance and versatility of the solver for RCS analysis three representative computer platforms have been chosen. The computer platforms are presented in the following list:

- **Personal Laptop:** Dual core Intel I5 processor (2.53 GHz) with 4 GB RAM and 300 GB of hard disk.
- **Medium range cluster (HPC):** Six nodes cluster with 2-way quad-core processors Intel Xeon E5620 (2.4 GHz, 12 Mb cache, 5.86 GT/s). Each node has 32 GB RAM and 250 GB of hard disk.

- **Shanghai Supercomputer Center (SSC):** A 35 nodes cluster with a total of 560 AMD CPUs: 16 CPU cores on each node and 4 GB RAM per core, and a total of RAM approximately equal to 2.24 TB. No hard disk storage is available for computations.

### 3.1. Metallic Benchmarks

To validate the results given by the solver, three RCS targets have been simulated and the simulation data have been compared with measurements. The fulfilled benchmarks have consisted of the monostatic analysis of the well-known metallic NASA Almond, the ogive and the cone-sphere at different frequencies obtaining results closely matched to the measurements shown in [51].

The monostatic analysis of the NASA Almond at several frequencies has been considered first. The parametric equations that define the geometry of the NASA Almond are well-known and available in the literature (for instance, [51]). The input mesh to the solver is the one shown in Figure 2.

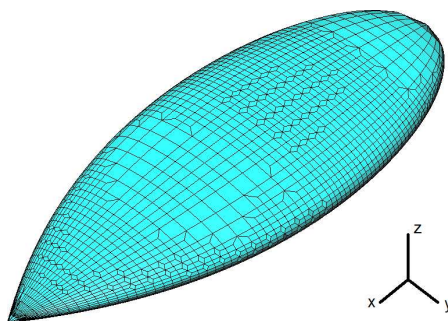


**Figure 2.** Input mesh to the solver for the NASA almond.

It is worth nothing that the same mesh can be used for different frequencies as the solver internally chooses the polynomial order and refines the mesh (if needed), in order to keep the dispersion error under control.

The three computer platforms described above have been used depending mainly on the frequency of analysis. Thus, the analysis at 1.19 GHz and 9.92 GHz has been run on the personal laptop. However, the memory requirements of the analysis at 21 GHz made the simulation impossible to be performed using the parallel in-core solver. Then, the HPC platform was used to run the simulation at that frequency. The comparison between the computed results and the measurements for 1.19 GHz and 9.92 GHz are shown in Figures 3

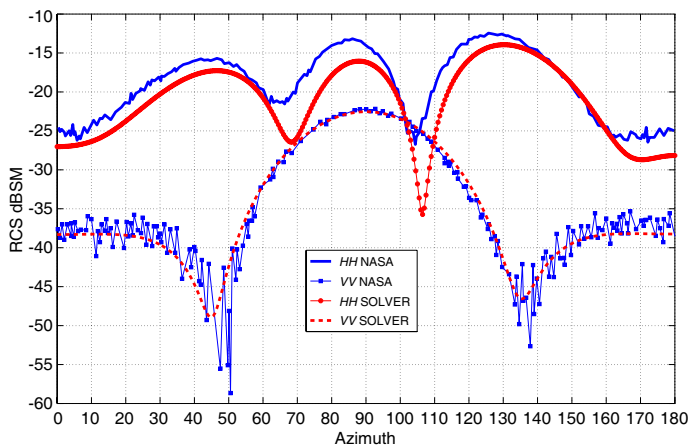


**Figure 3.** Radar cross-section of NASA almond at 1.19 GHz.

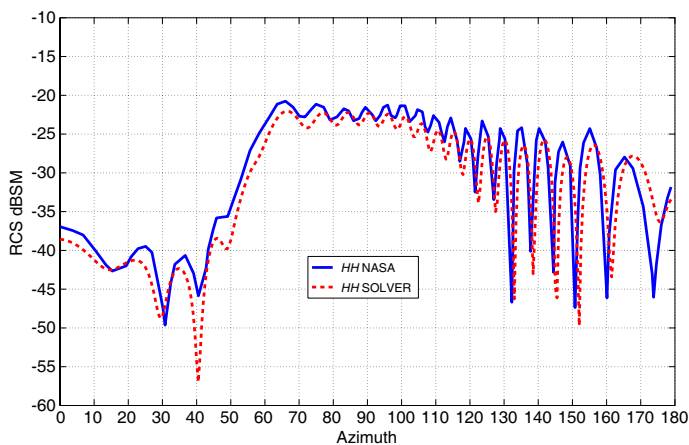


**Figure 4.** Radar cross-section of NASA almond at 9.92 GHz.

and 4, respectively. However, as there is no measurement for 21 GHz, the computed results at that frequency have been compared with other numerical results published in the literature [52]. An excellent agreement is observed despite the fact the differences between both numerical techniques (see Figure 5).

At this point, it is worth nothing that is possible to run the analysis at 21 GHz on the personal laptop; but using the parallel out-of-core version of the solver. However, the main constraint of the out-of-core solver using a single computer is the time required for each simulation as it will be illustrated later.

**Table 1.** Limits of each computer platform for the monostatic analysis of the NASA almond.

Solver	Simulation Data	Computer Platforms		
		Laptop	HPC	SSC
In core	DoF	15.000	110.000	370.000
	Time	0.607 hours	7.3 hours	19 hours
	Freq.	13 GHz	75 GHz	150 GHz
	Memory	3.6 GB	193.6 GB	2.24 TB
Out of core	DoF	110.000	283.000	
	Time	≈ 8 days	≈ 4 days	
	Freq.	75 GHz	130 GHz	
	Hard Disk	193.6 GB	1.28 TB	

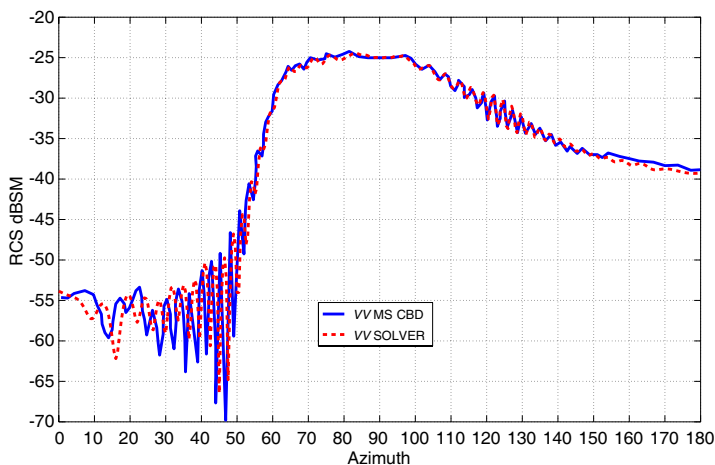


**Figure 5.** Radar cross-section of NASA almond at 21 GHz.

The above considerations relative to the limits of each computer platform in terms of the size of the problem (i.e., the highest frequency of the analysis) for the in-core version of the solver are gathered in Table 1 in a row wise. Thus, by shifting to the right in the table, it is observed how the solver is able to run either a larger problem or a given fixed size problem much faster. Table 1 gathers also limits for the out-of-core version of the solver. The limit with the out-of-core version is reached when all available disk storage is used for computation. Thus, the maximum frequency of the analysis is 130 GHz for the HPC cluster and 75 GHz for the laptop. Note that no data is included in the table for the limit with the SSC system. This is due simply because, in

that system, the hard disk is not available for computational purposes. However, in most cases, there is no much sense of using the out-core version on a supercomputer. It must be remarked that in some situations the limit in practice for the out-of-core version is not due to the available hard disk in the system but to the time the users are willing to wait for a simulation. Thus, an 8 days simulation on a laptop seems to exceed reasonable limits. Considering a 24 hours limit, the highest frequency of analysis in the laptop is reduced to 43 GHz (corresponding to approximately 50.000 degrees of freedom).

As it is shown in the table, the limit of the SSC system for the NASA Almond is at 150 GHz. In this case, instead of running this model at that frequency, another example has been chosen in order to compare with available results. The case considered is the bistatic analysis at 8 GHz of a scatterer similar to the NASA Almond of previous results but with a total length of 2.5 meters. The target is illuminated by an incident plane wave along the  $x$ -axis (vertical and horizontal polarizations are considered). The number of degrees of freedom of this problem is around 315.000 and the simulation time is 12.2 hours using the SSC system. The results of both polarizations (labeled as  $HH$  for horizontal and  $VV$  for vertical) are shown in Figure 6.

Finally, the monostatic analysis of the ogive and the cone-sphere shown in [51] are considered. The comparison between the computed results and the measurements for the ogive target at 1.18 GHz and for the cone-sphere target at 9 GHz are shown in Figures 7 and 8. Again there is an excellent agreement with the measurements in both cases.

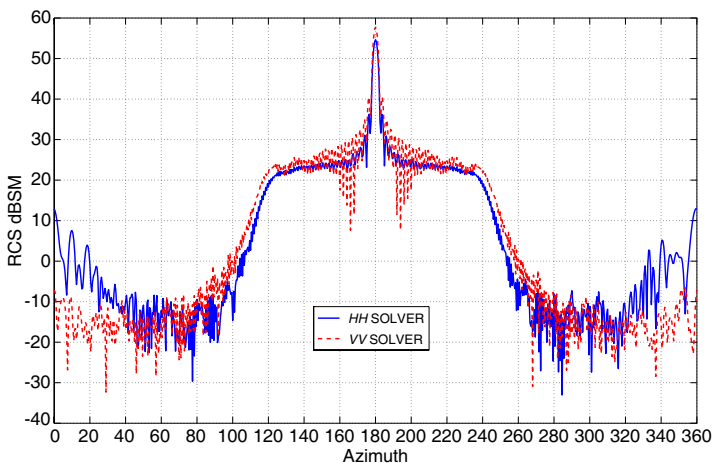


**Figure 6.** Bistatic RCS of JINA 2006 almond at 8 GHz.

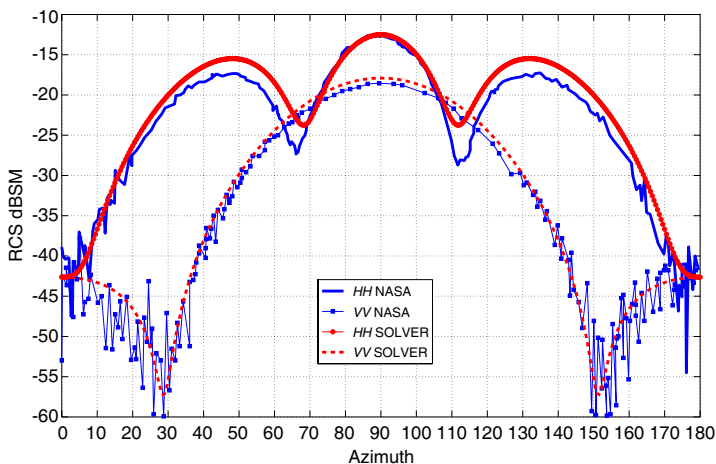


Figure 7. RCS of single metallic ogive at 1.18 GHz.

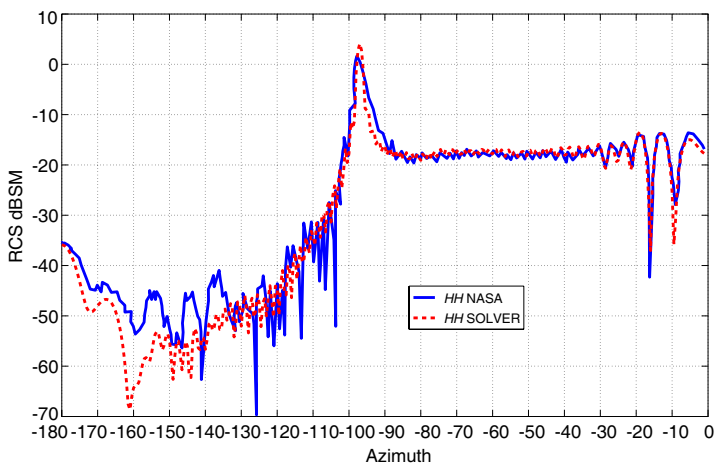
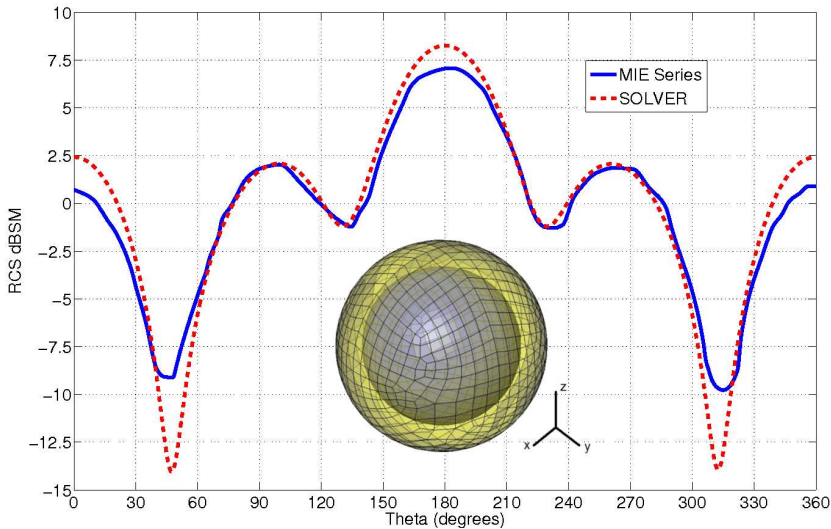


Figure 8. Monostatic RCS of metallic cone-sphere at 9 GHz.

### 3.2. Metallo-dielectric Benchmarks

To validate the results given by the solver using dielectric materials, two dielectric coated targets have been simulated. The benchmarks have consisted of the bistatic analysis of a conducting sphere with a dielectric coating and the monostatic analysis of a coated NASA almond. The input mesh to the solver for these two structures are shown as insets in Figures 9 and 10.

The bistatic analysis of the conducting sphere covered by a



**Figure 9.** Bistatic RCS ( $\theta\theta$  polarization) of a coated sphere ( $r_1 = 0.3$  m,  $r_2 = 0.4$  m,  $\epsilon_r = 3$ ).

dielectric shell has been carried out using the personal laptop. The total number of degrees of freedom of this problem is 4752. The internal radius of the sphere is  $r_1 = 0.3$  m, the external radius is  $r_2 = 0.4$  m and the permittivity of the dielectric shell with respect to vacuum medium is  $\epsilon_r = 3$ . The sphere is illuminated by an incident plane wave along the  $z$ -axis ( $\theta\theta$  polarization). The incident frequency is 300 MHz. The computed results of this analysis have been compared with the results given by the MIE series solution. The comparison between both results is shown in Figure 9. Again, the comparison presents a good agreement between both results.

The monostatic analysis of the coated NASA almond has been carried out using the HPC platform. In this case,  $\theta\theta$  polarization and  $\phi\phi$  polarization have been considered. The incident frequency is 3 GHz and the thickness of the coating is 10 mm. For this analysis, as there is no measurement to compare the results, three different simulations have been performed to validate the computed results. The simulations have consisted of the analysis of the metallic NASA almond, the coated NASA almond using air as dielectric shell ( $\epsilon_r = 1$ ,  $\mu_r = 1$ ) and the coated NASA almond using a lossy dielectric shell ( $\epsilon_r = 3 - 2i$ ,  $\mu_r = 2 - i$ ). The case of adding a shell with  $\epsilon_r = 1$ ,  $\mu_r = 1$  is for validation purposes. As it is expected, the results of the metallic NASA almond and the coated NASA almond for this case show a perfect agreement. The results of these simulations are shown

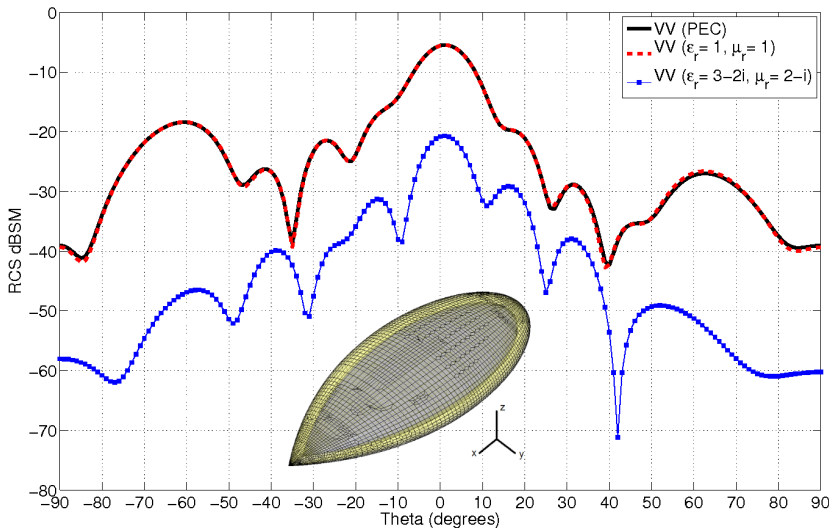


**Figure 10.** Monostatic RCS of coated NASA almond at 3 GHz in upper  $x$ - $z$  plane for vertical polarization).

in Figure 10 for both polarizations. It is observed the effect of the electric and magnetic losses in the reduction of the RCS.

### 3.3. Realistic Benchmark

This benchmark has consisted of the bistatic analysis of the helicopter shown as inset in Figure 11. The wheels and the blades of this helicopter have been considered as dielectric to make a realistic model. A  $\epsilon_r = 4.5$  has been chosen since the values of  $\epsilon_r$  for different materials, mainly carbon and glass fibers, are around 4.5.

The simulation of this benchmark has been performed on SSC platform. The operating frequency is 800 MHz. The helicopter model is 17.7 m long, 14.6 m wide and 3.8 m high. The corresponding electrical sizes of the model are  $47.2\lambda$ ,  $38.93\lambda$  and  $10.13\lambda$ , where  $\lambda$  is the free-space wavelength at the operating frequency. The helicopter is illuminated by an incident plane wave with  $\theta\theta$  polarization along the  $-y$ -axis.

The total number of degrees of freedom for the accurate modeling of this problem was around 255000 (half in the case of no dielectric parts in the model). The total RAM memory needed to solve this problem was 968.94 GB and the simulation took 9.67 hours. The computed results for azimuth angle are shown in Figure 11. The main lobe of the RCS appears in the tail of the helicopter ( $\phi = 270^\circ$ ), while

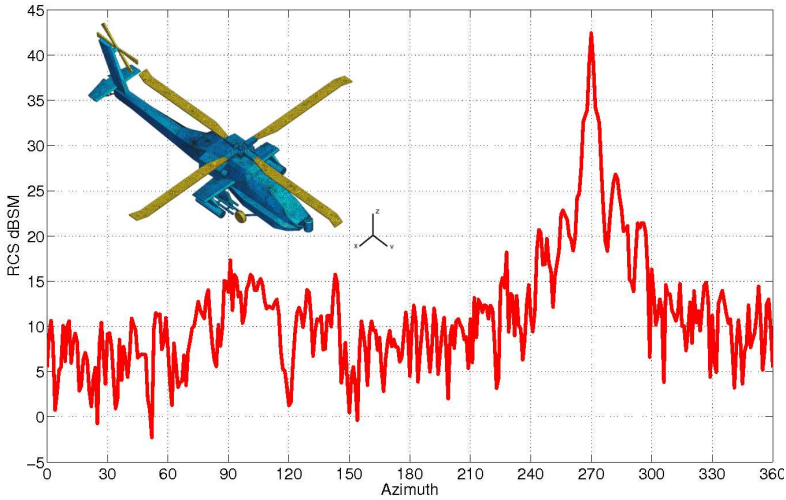


**Figure 11.** Bistatic RCS of real helicopter at 800 MHz in azimuth.

the incident plane wave is coming from  $\phi = 90^\circ$ .

Finally, in order to illustrate the capabilities of the out-of-core solver in a realistic problem, the out-of-core simulation of the helicopter has been performed in the HPC platform. It is worth reminding here that the SSC platform has no hard-disk storage available for computations. Thus, the direct comparison between the performance of the solver in both versions, in-core and out-of-core, is not possible. However, the HPC platform is representative of an affordable computer system for research/development groups. Furthermore, the out-of-core analysis of the helicopter in such HPC system has resulted to be a close limit (see Table 1) of what could be run in a medium range cluster. Specifically, the out-of-core simulation of the helicopter used all the RAM memory available in the HPC cluster (193.6 GB) and around 1.0 TB of hard disk. The simulation took almost 3 days (70.2 hours).

#### 4. CONCLUSIONS

The RCS analysis of several benchmark structures has been performed using a parallel direct solver. In-core and out-of-core versions of the solver have been used on three representative computer platforms. The results obtained have shown the reliability, performance and versatility of the code that has run on a wide variety of computer platforms, going from a single-user laptop to a supercomputer. The results have shown to be illustrative of what is the maximum frequency of analysis of the structures for a given type of simulation platform.

## ACKNOWLEDGMENT

The authors want to thank the Shanghai Supercomputer Center for providing access to its computational resources. The authors would like also to acknowledge the support of Ministerio de Educación y Ciencia of Spain under project TEC2010-18175/TCM.

## REFERENCES

1. Ludwig, A. C., "Computation of radiation patterns involving numerical double integration," *IEEE Transactions on Antennas and Propagation*, Vol. 16, 767–769, Nov. 1968.
2. Ufimtsev, P. Y., *Theory of Edge Diffraction in Electromagnetics*, Tech Science Press, 2003.
3. Moschovitis, C. G., H. Anastassiou, and P. V. Frangos, "Scattering of electromagnetic waves from a rectangular plate using an extended stationary phase method based on Fresnel functions (SPM-F)," *Progress In Electromagnetics Research*, Vol. 107, 63–99, 2010.
4. Keller, J. B., "Geometrical theory of diffraction," *Journal of the Optical Society of America*, 1962.
5. Kouyoumjian, R. G. and P. H. Pathak, "A uniform geometrical theory of diffraction for an edge in a perfectly conducting surface," *Proceedings of the IEEE*, 1448–1461, Nov. 1974.
6. Ling, H., R.-C. Chou, and S.-W. Lee, "Shooting and bouncing rays: Calculating the RCS of an arbitrarily shaped cavity," *IEEE Transactions on Antennas and Propagation*, Vol. 37, 194–205, Feb. 1989.
7. Harrington, R. F., *Field Computation by Moment Methods*, IEEE Press, 1993.
8. Jin, J. M., *The Finite Element Method in Electromagnetics*, 2nd edition, John Wiley & Sons, Inc., 2002.
9. Salazar-Palma, M., T. K. Sarkar, L. E. García-Castillo, T. Roy, and A. R. Djordjevic, *Iterative and Self-adaptive Finite-elements in Electromagnetic Modeling*, Artech House Publishers, Inc., Norwood, MA, 1998.
10. Taflov, M., *Advances in Computational Electrodynamics: The Finite-difference Time-domain Method*, Artech House Publishers, Inc., 1998.
11. Ilic, M., M. Djordjevic, A. Ilic, and B. Notaros, "Higher order hybrid FEM-MoM technique for analysis of antennas and

- scatterers,” *IEEE Transactions on Antennas and Propagation*, Vol. 57, 1452–1460, May 2009.
12. Chen, M., Y. Zhang, X. W. Zhao, and C. H. Liang, “Analysis of antenna around NURBS surface with hybrid MoM-PO technique,” *IEEE Transactions on Antennas and Propagation*, Vol. 55, 407–413, Feb. 2007.
  13. Becker, A. and V. Hansen, “A hybrid method combining the multitemporal resolution time-domain method of moments with the time-domain geometrical theory of diffraction for thin-wire antenna problems,” *IEEE Transactions on Antennas and Propagation*, Vol. 54, 953–960, Mar. 2006.
  14. Fernandez-Recio, R., L. E. García-Castillo, I. Gomez-Revuelto, and M. Salazar-Palma, “Fully coupled hybrid FEM-UTD method using NURBS for the analysis of radiation problems,” *IEEE Transactions on Antennas and Propagation*, Vol. 56, 774–783, Mar. 2008.
  15. Gomez-Revuelto, I., L. E. García-Castillo, M. Salazar-Palma, and T. K. Sarkar, “Fully coupled hybrid method FEM/high-frequency technique for the analysis of radiation and scattering problems,” *Microwave and Optical Technology Letters*, Vol. 47, 104–107, Oct. 2005.
  16. Liu, Z.-L. and J. Yang, “Analysis of electromagnetic scattering with higher-order moment method and NURBS model,” *Progress In Electromagnetics Research*, Vol. 96, 83–100, 2009.
  17. Wang, S., X. Guan, D.-W. Wang, X. Ma, and Y. Su, “Electromagnetic scattering by mixed conducting/dielectric objects using higher-order MoM,” *Progress In Electromagnetics Research*, Vol. 66, 51–63, 2006.
  18. Lai, B., N. Wang, H.-B. Yuan, and C.-H. Liang, “Hybrid method of higher-order MoM and Nyström discretization PO for 3D PEC problems,” *Progress In Electromagnetics Research*, Vol. 109, 381–398, 2010.
  19. Coifman, R., V. Rokhlin, and S. Wandzura, “The fast multipole method for the wave equation: A pedestrian prescription,” *IEEE Antennas and Propagation Magazine*, Vol. 35, 7–12, Jun. 1993.
  20. Phillips, J. R. and J. K. White, “A precorrected-FFT method for electrostatic analysis of complicated 3-D structures,” *IEEE Transactions on Computer Aided Design Integrated Circuits*, Vol. 16, 1059–1072, Oct. 1997.
  21. Bleszynski, E., M. Bleszynski, and T. Jaroszewicz, “AIM: Adaptive integral method for solving large-scale electromagnetic scattering and radiation problems,” *Radio Science*, Vol. 31, No. 5,

- 1225–1251, 1996.
22. Hu, L., L.-W. Li, and T. S. Yeo, “Analysis of scattering by large inhomogeneous bi-anisotropic objects using AIM,” *Progress In Electromagnetics Research*, Vol. 99, 21–36, 2009.
  23. Seo, S. M. and J. F. Lee, “A fast IE-FFT algorithm for solving PEC scattering problems,” *IEEE Transactions on Magnetics*, Vol. 41, 1476–1479, May 2005.
  24. Taboada, J. M., M. G. Araujo, J. M. Bertolo, L. Landesa, F. Obelleiro, and J. L. Rodriguez, “MLFMA-FFT parallel algorithm for the solution of large-scale problems in electromagnetics,” *Progress In Electromagnetics Research*, Vol. 105, 15–30, 2010.
  25. Seo, S. M. and J. F. Lee, “A single level low rank IE-QR algorithm for PEC scattering problems using EFIE formulation,” *IEEE Transactions on Antennas and Propagation*, Vol. 52, 2141–2146, Aug. 2004.
  26. Bebendorf, M., “Approximation of boundary element matrices,” *Numerische Mathematik*, Vol. 86, No. 4, 565–589, 2000.
  27. Zhao, K., M. N. Vouvakis, and J.-F. Lee, “The adaptive cross approximation algorithm for accelerated method of moments computations of EMC problems,” *IEEE Transactions on Electromagnetic Compatibility*, Vol. 47, Nov. 2005.
  28. Hackbusch, W., “A sparse matrix arithmetic based on  $H$ -matrices. Part I: Introduction to  $H$ -matrices,” *Computing*, Vol. 62, No. 2, 89–108, 1999.
  29. Bebendorf, M. and W. Hackbusch, “Existence of  $H$ -matrix approximants to the inverse  $FE$ -matrix of elliptic operators with  $L$ -infinity-coefficients,” *Numerische Mathematik*, Vol. 95, No. 1, 1–28, 2003.
  30. Michielssen, E. and A. Boag, “A multilevel matrix decomposition algorithm for analyzing scattering from large structures,” *IEEE Transactions on Antennas and Propagation*, Vol. 44, 1086–1093, Aug. 1996.
  31. Rius, J., J. Parron, A. Heldring, J. Tamayo, and E. Ubeda, “Fast iterative solution of integral equations with method of moments and matrix decomposition algorithm; singular value decomposition,” *IEEE Transactions on Antennas and Propagation*, Vol. 56, 2314–2324, Aug. 2008.
  32. Vion, A., R. V. Sabariego, and C. Geuzaine, “A model reduction algorithm for solving multiple scattering problems using iterative methods,” *IEEE Transactions on Magnetics*, Vol. 47, No. 5, 1470–1473, 2011.

33. Prakash, V. and R. Mittra, "Characteristic basis function method: A new technique for efficient solution of method of moment matrix equations," *Microwave and Optical Technology Letters*, Vol. 36, 95–100, Jan. 2003.
34. Delgado, C., M. Catedra, and R. Mittra, "Efficient multilevel approach for the generation of characteristic basis functions for large scatters," *IEEE Transactions on Antennas and Propagation*, Vol. 56, 2134–2137, Jul. 2008.
35. Shifman, Y. and Y. Leviatan, "Scattering by a groove in a conducting plane — A PO-MoM hybrid formulation and wavelet analysis," *IEEE Transactions on Antennas and Propagation*, Vol. 49, 1807–1811, Dec. 2001.
36. Dai, S. Y., C. M. Zhang, and Z. S. Wu, "Electromagnetic scattering of objects above ground using MRTD/FDTD hybrid method," *Journal of Electromagnetic Waves and Applications*, Vol. 23, No. 16, 2187–2196, 2009.
37. Shaeffer, J., "Direct solve of electrically large integral equations for problem sizes to 1 M unknowns," *IEEE Transactions on Antennas and Propagation*, Vol. 56, 2306–2313, Aug. 2008.
38. Lucente, E., A. Monorchio, and R. Mittra, "An iteration-free MoM approach based on excitation independent characteristic basis functions for solving large multiscale electromagnetic scattering problems," *IEEE Transactions on Antennas and Propagation*, Vol. 56, 999–1007, Apr. 2008.
39. Heldring, A., J. Rius, J. Tamayo, J. Parro, and E. Ubeda, "Multiscale compressed block decomposition for fast direct solution of method of moments linear system," *IEEE Transactions on Antennas and Propagation*, Vol. 59, 526–536, Feb. 2011.
40. Zhang, Y., M. Taylor, T. Sarkar, H. Moon, and M. Yuan, "Solving large complex problems using a higher-order basis: Parallel in-core and out-of-core integral-equation solvers," *IEEE Antennas and Propagation Magazine*, Vol. 50, No. 4, 13–30, 2008.
41. García-Donoro, D., Y. Zhang, W. Zhao, T. K. Sarkar, L. E. García-Castillo, and M. Salazar-Palma, "HOBBIES: Higher order basis based integral equation solver with automatic goal oriented optimization," *CEFC 2010*, Chicago, Illinois, USA, May 2010.
42. Zhang, Y., M. Taylor, T. Sarkar, A. De, M. Yuan, H. Moon, and C. Liang, "Parallel in-core and out-of-core solution of electrically large problems using the RWG basis functions," *IEEE Antennas and Propagation Magazine*, Vol. 50, No. 5, 84–94, 2008.
43. Zhang, Y., R. van de Geijn, M. Taylor, and T. Sarkar, "Parallel

- MoM using higher-order basis functions and LAPACK in-core and out-of-core solvers for challenging EM simulations,” *IEEE Antennas and Propagation Magazine*, Vol. 51, No. 5, 42–60, 2009.
44. Li, L.-W., Y.-J. Wang, and E.-P. Li, “MPI-based parallelized precorrected FFT algorithm for analyzing scattering by arbitrarily shaped three-dimensional objects,” *Progress In Electromagnetics Research*, Vol. 42, 247–259, 2003.
  45. Zhang, Y., J. Porter, M. Taylor, and T. Sarkar, “Solving challenging electromagnetic problems using MoM and a parallel out-of-core solver on high performance clusters,” *IEEE Antennas and Propagation Society International Symposium 2008, AP-S 2008*, 1–4, 2008.
  46. Harrington, R. F., “Boundary integral formulations for homogeneous material bodies,” *Journal of Electromagnetic Waves and Applications*, Vol. 3, No. 1, 1–15, 1989.
  47. Rao, S. M., C. C. Cha, R. L. Cravey, and D. L. Wilkes, “Electromagnetic scattering from arbitrary shaped conducting bodies coated with lossy material of arbitrary thickness,” *IEEE Transactions on Antennas and Propagation*, Vol. 3, No. 1, 1–15, 1989.
  48. Zhang, Y. and T. K. Sarkar, *Parallel Solution of Integral Equation Based EM Problems in the Frequency Domain*, Wiley-IEEE Press, Jul. 2009.
  49. “Message passing interface forum,” <http://www.mpi-forum.org/>.
  50. “The ScaLAPACK project,” <http://www.netlib.org/scalapack/>.
  51. Woo, A., H. Wang, M. Schuh, and M. Sanders, “EM programmer’s notebook. Benchmark radar targets for the validation of computational electromagnetics programs,” *IEEE Antennas and Propagation Magazine*, Vol. 35, 84–89, Feb. 1993.
  52. Heldring, A., J. M. Rius, and J. M. Tamayo, “Direct MoM solution of electrically large problems with  $N^2$  complexity,” *2010 Proceedings of the Fourth European Conference on Antennas and Propagation (EuCAP)*, 1–4, 2010.